Molecular and Cell Biotechnologies

https://doi.org/10.7124/bc.000B3F
UDC 577.322:004.94:578.834.1:615.277

N.V. Khmil[1, 2], A.V. Shestopalova[1]

[1] O.Ya. Usikov Institute for Radiophysics and Electronics, NAS of Ukraine
12, Akademika Proskura Str., Kharkov, Ukraine, 61085
[2] Kharkiv National University of Radio Electronics
14, Nauky Ave., Kharkiv, Ukraine, 61166
nataliia.khmil@nure.ua

EFFECT OF ANTIVIRALS AND A PEPTIDOMIMETIC INHIBITOR ON FURIN CONFORMATIONAL STABILITY: MOLECULAR DOCKING AND MOLECULAR DYNAMICS SIMULATIONS

Furin is a key host protease involved in proteolytic activation of the SARS-CoV-2 spike protein (S protein) at the S1/S2 cleavage site, thereby facilitating membrane fusion, making it an attractive target for the antiviral drug development. ***Aim.*** *To evaluate the conformational stability and binding behavior of furin in a complex with nelfinavir, remdesivir and the macrocyclic peptidomimetic inhibitor 8 (PI8) using computational approaches.* ***Methods.*** *Molecular docking and 100-ns molecular dynamics (MD) simulations were used to characterize ligand-binding modes and assess the structural stability of furin-ligand complexes.* ***Results.*** *Docking analysis identified PI8 as the energetically most favorable compound (–9.1 kcal/mol) that forms stable interaction within the catalytic site, while nelfinavir and remdesivir showed slightly lower affinities (–8.7 and –8.9 kcal/mol, respectively). MD simulations confirmed the structural stability of all complexes over the 100-ns trajectory, supporting the reliability of the predicted binding modes.* ***Conclusions.*** *Molecular docking and MD approach provide a robust framework for identifying and characterizing potential furin inhibitors.*

Keywords: *furin, antivirals, macrocyclic peptidomimetic inhibitor 8, SARS-CoV-2 S protein, molecular docking, molecular dynamics simulation.*

Citation: Khmil N.V., Shestopalova A.V. (2026) Effect of antivirals and a peptidomimetic inhibitor on furin conformational stability: Molecular docking and molecular dynamics simulations. *Biopolymers & Cell*, 2(42), 129—138. https://doi.org/10.7124/bc.000B3F

Introduction

Coronavirus disease 2019 (COVID-19), caused by severe acute respiratory syndrome coronavirus 2 (SARS-CoV-2), continues to affect global health, with over 7 million deaths reported worldwide by February 2026 (https://covid19.who.int/). In Ukraine, Omicron subvariants predominate, including recombinant forms and recently identified strains such as Stratus (XFG) and Nimbus (NB.1.8.1), although their confirmed incidence remains limited (https://phc.org.ua).

The SARS-CoV-2 S protein mediates host-cell recognition via the S1 subunit and membrane fusion via the S2 subunit. The S1 receptor-binding domain interacts with the ACE2 receptor [1—3]. Viral entry requires proteolytic activation at the S1/S2 and S2' sites by host proteases, including furin and TMPRSS2 [4, 5], while the polybasic furin cleavage site enhances infectivity and transmissibility [6]. Furin is a calcium-dependent serine endoprotease involved in the processing of numerous precursor proteins and viral substrates [7—13], and contains a catalytic domain with the Ser368–His194–Asp153 triad [14—17]. In addition, cathepsins may also be involved in the proteolytic activation of the SARS-CoV-2 S protein [18, 19]. Given its role in viral entry, furin is a promising antiviral target [20]. Several inhibitors and repurposed drugs have been explored [21—28], but their involvement in essential physiological processes raises concerns about potential side effects, emphasizing the need to understand ligand-binding mechanisms and their stability [29].

Therefore, the aim of this study was to investigate the binding modes and conformational stability of furin in complex with nelfinavir, remdesivir, and PI8 using molecular docking and MD simulations.

Materials and Methods

Preparation of protein and ligands

The 3D structure of furin (PDB ID: 5JXG) was downloaded from the RCSB Protein Data Bank, corresponding to the soluble ectodomain (~581 residues) that lacks the C-terminal transmembrane helix and cytoplasmic tail present in the full-length protein [14]. Remdesivir and nelfinavir structures were retrieved from the PubChem database in SDF format; PI8 structure was obtained from the protein database in PDB format (https://www.rcsb.org/ligand/PI8). Ligands were energy minimized using the Universal Force Field and converted to PDBQT format with AutoDockTools (v1.5.6) [30]. The protein preparation involved the removal of water molecules and the assignment of protonation states at pH 7.4. Hydrogen atoms and Gasteiger charges were also added. Molecular docking was performed using a grid box of 70 × 70 × 70 Å centered at x = –35.258, y = –37.758, z = 0.284, with an exhaustiveness of 50 and a grid spacing of 0.508 Å.

Molecular docking analysis

Molecular docking was performed using AutoDock Vina (v1.1.2) [31,32]. To validate these results, an independent docking approach was applied using the CB-Dock2 web server. The complexes with the highest affinity scores were visualized and analyzed for non-covalent interactions using PyMOL (v2.5) [33] and the Discovery Studio 2024 Client software [34]. Docking reliability was assessed by redocking the furin-ligand complexes; the root mean square deviation between the crystallographic and redocked poses was below 2 Å, confirming the accurate reproduction of the binding modes.

MD simulations

MD simulations of furin-ligand complexes were performed using GROMACS (v2024.4) with the CHARMM27 force field [35]. Ligand topologies were generated using the SwissParam server [36]. The systems were solvated with the TIP3P water model and neutralized by adding Na^+ and Cl^- ions. Long-range electrostatics were treated with the Particle Mesh Ewald method with a cutoff of 1.2 nm, while van der Waals interactions were switched off between 1.0 and 1.2 nm [37]. Energy minimization was followed by equilibration under

NVT conditions (1.1 ns, 300 K) using the V-rescale thermostat, and subsequently under NPT conditions with the V-rescale thermostat and the Berendsen barostat. MD simulations were conducted for 100 ns with a time step of 2 fs at 300 K and 1 bar. Trajectory analysis included root mean square deviation (RMSD), root mean square fluctuation (RMSF), radius of gyration (Rg) of Cα atoms, and hydrogen bond formation, calculated using standard GROMACS tools. Figures were generated from .xvg outputs.

Results and Discussion

Molecular docking

AutoDock Vina and CB-Dock2 provided consistent ligand orientations and binding site predictions [38]. AutoDock Vina predicted binding energies of –9.1 kcal/mol (PI8), –8.7 kcal/mol (nelfinavir), and –8.9 kcal/mol (remdesivir), while CB-Dock2 yielded comparable values of –8.8, –8.2, and –8.5 kcal/mol, respectively. The most favorable binding conformations are shown in Fig. 1.

PI8 is a macrocyclic peptidomimetic inhibitor (https://www.chemspider.com/Chemical-Structure.392745.html) designed to target the enzymatic activity of proprotein convertases, representing an alternative to classical peptide-based furin inhibitors [39—41]. In addition, PI8 exhibits inhibitory activity against HIV proteases, highlighting its potential as a broad-spectrum protease inhibitor [42]. PI8 demonstrated the highest binding affinity to furin, with an AutoDock Vina score of –9.1 kcal/mol, binding within the catalytic site (Fig. 1*a*). It formed hydrogen bonds with Pro266, Glu271, and Ser311, hydrophobic interactions with Ala267, Arg268, Ile312, and Tyr313, as well as van der Waals contacts and a π-cation interaction with Arg490 (Fig. 1*b*). Blind docking yielded a comparable binding energy (–8.8 kcal/mol), with hydrogen bonding to Arg490, π-anion interaction with Asp530, and π-stacking with Phe275 and Trp531 (Fig. 1*c*). These interactions support preferential localization of PI8 within the catalytic domain, contributing to its high affinity.

Comparison with nelfinavir and remdesivir revealed similar binding orientations within the catalytic site (Fig. 1*d*, Fig. 1*g*). Remdesivir retained hydrogen bonds with Pro266 and Glu271 and hydrophobic contacts with Arg268, Ile312, and Trp531, occupying pockets corresponding to the S4 and S5 subsites [40]. Nelfinavir exhibited π-stacking with Trp531, whereas remdesivir formed a π-cation interaction with Arg490 (Fig. 1*e*, Fig. 1*h*). Their binding energies were slightly lower (–8.7 and –8.9 kcal/mol, respectively). In blind docking, the stabilization of nelfinavir and remdesivir complexes was also supported by π-stacking interactions with aromatic residues such as Phe275 and Trp531, similar to PI8, indicating their role in ligand positioning within the binding cavity (Fig. 1*f*, Fig. 1*i*). CB-Dock2 predicted binding affinities of –8.2 kcal/mol (nelfinavir) and –8.5 kcal/mol (remdesivir).

Nelfinavir, originally developed as an HIV-1 protease inhibitor, has been shown to inhibit host proteases, including furin [43—45]. Remdesivir, a nucleotide analog targeting viral RNA-dependent RNA polymerase, is less hydrophobic and richer in heteroatoms compared to nelfinavir, that may influence its binding profile [46, 47]. Their structural diversity and distinct mechanisms make them suitable for the comparative docking analysis together with PI8.

Molecular dynamics

The RMSD profiles of Cα atoms over 100 ns for apo furin and its complexes with nelfinavir, remdesivir, and PI8 are presented in Fig. 2.

All systems show a rapid increase in RMSD during the first 5—10 ns, followed by equilibration. Apo furin exhibits the lowest RMSD (0.12—0.15 nm), indicating high stability. The nelfinavir complex shows a gradual increase after ~50 ns (0.20—0.22 nm), suggesting ligand-induced conformational changes, while remdesivir (0.15—0.18 nm) and PI8 (0.16—0.19 nm) remain stable with minor fluctuations.

RMSF analysis shows generally low flexibility (RMSF < 0.2 nm), confirming the preservation of the global fold (Fig. 3). Increased fluctuations are

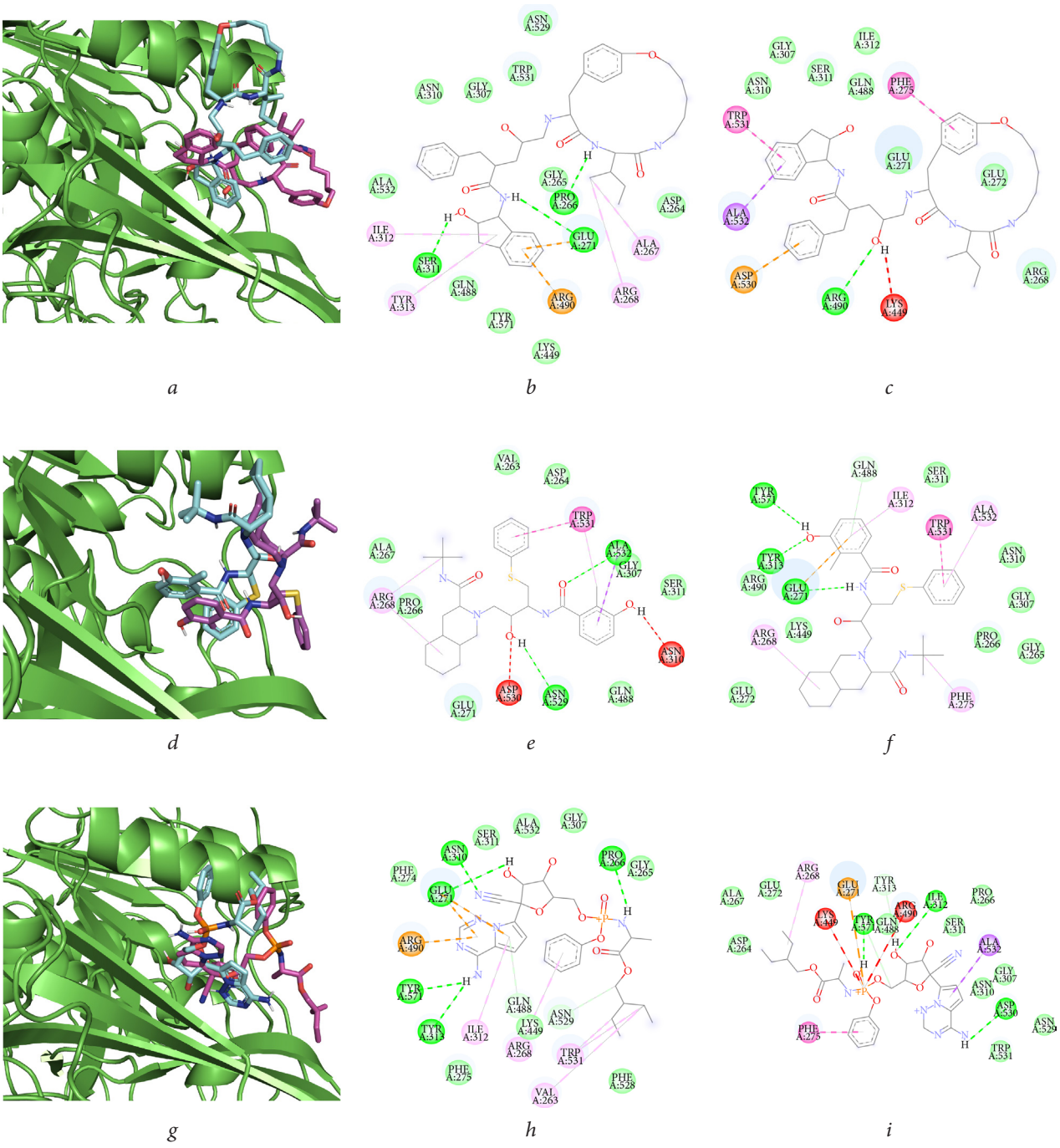

Fig. 1. Binding modes of potential inhibitors predicted by AutoDock Vina and CB-Dock2. The top-ranked poses are shown in magenta (AutoDock Vina) and cyan (CB-Dock2): *a*, *b*, *c* — PI8, *d*, *e*, *f* — nelfinavir, *g*, *h*, *i* — remdesivir. Panels (*b*, *e*, *h*) and (*c*, *f*, *i*) represent Discovery Studio visualizations for AutoDock Vina and CB-Dock2 results, respectively. The furin structure is shown as green ribbons. For all panels, the 2D interaction diagrams (center and right column) are presented in color: — van der Waals; — hydrogen bond; — π-anion, π-cation; — alkyl; — π-sigma; — π-stacked; — unfavorable donor-donor

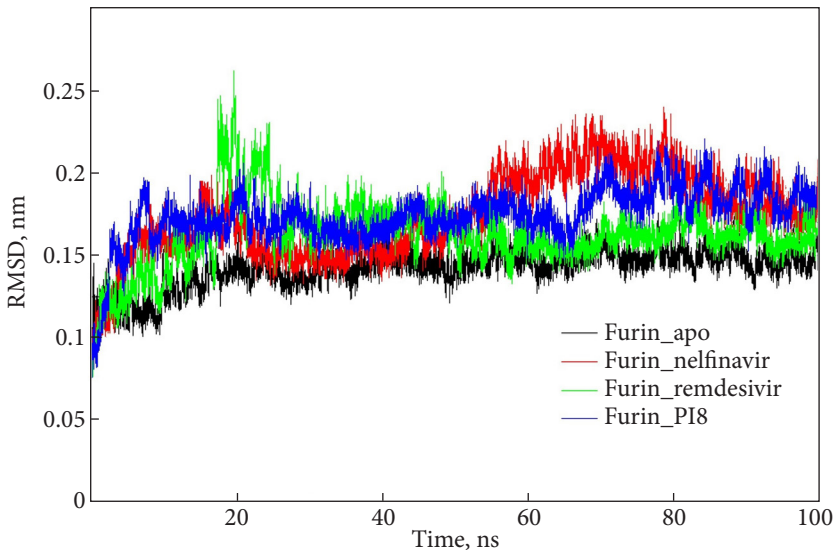

Fig. 2. Root mean square deviation of Cα atoms of furin in the apo form and in complexes with remdesivir, nelfinavir, and PI8 over 100 ns MD simulations

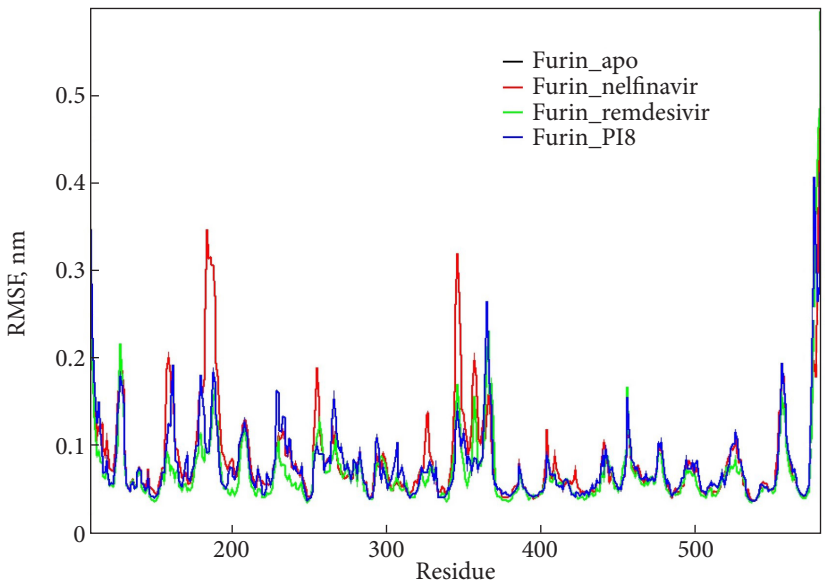

Fig. 3. Root mean square fluctuation of Cα atoms of furin in the apo form and in complexes with remdesivir, nelfinavir, and PI8 over 100 ns MD simulations

observed in nelfinavir at residues 150—200 and 340—360, consistent with higher RMSD values, whereas remdesivir and PI8 remain similar to the apo form. The overall residue fluctuations remain below 0.5 nm, indicating the preservation of structural integrity and stability of the secondary structure.

Fig. 4 shows the intermolecular hydrogen bonds between furin and remdesivir, nelfinavir, and PI8 during 100 ns MD simulations. The nelfinavir complex exhibited the highest stability, maintaining 3—5 hydrogen bonds on average, while remdesivir formed 2—5 hydrogen bonds with moderate fluctuations. PI8 formed only 1—4 hydrogen bonds, indicating weaker polar interactions. Nevertheless, PI8 showed the most favorable docking score, suggesting that its binding affinity is largely driven by hydrophobic contacts with Ala267,

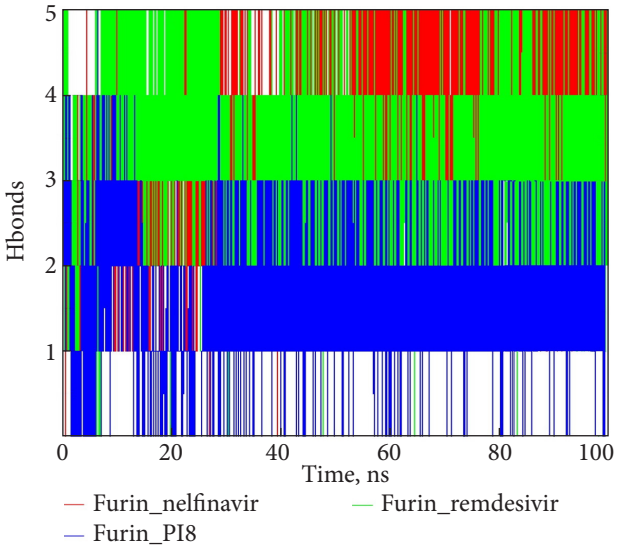

Fig. 4. Time evolution of intermolecular hydrogen bonds between furin and remdesivir, nelfinavir, and PI8 over 100 ns MD simulations

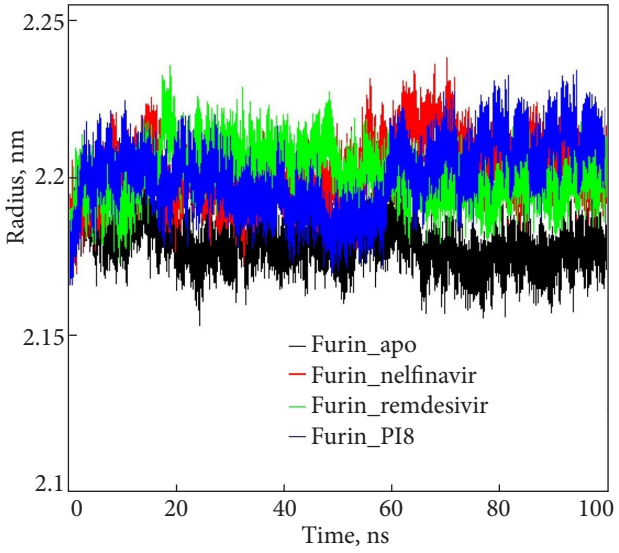

Fig. 5. Radius of gyration of Cα atoms of furin in the apo form and in complexes with remdesivir, nelfinavir, and PI8

Arg268, Ile312, and Tyr313, van der Waals interactions with Asn310 and Gly307, and favorable shape complementarity within the binding pocket.

All systems showed stable Rg values (2.16—2.22 nm), indicating preservation of the global fold (Fig. 5). The apo form had the lowest Rg (2.16—2.18 nm), reflecting a compact and stable structure. The nelfinavir complex exhibited slightly higher values (2.18—2.21 nm) with moderate fluctuations after ~50 ns, suggesting minor expansion. Remdesivir and PI8 complexes showed similar ranges (2.19—2.22 nm and 2.18—2.21 nm, respectively), indicating slightly less compact but equilibrated structures. Overall, these results agree with previous MD studies reporting Rg values around 2.2 nm for apo furin and inhibitor complexes [28].

Furin consists of signal peptide (1—26), a propeptide (27—107), a catalytic domain (108—292), a P domain (293—451), and a cysteine-rich region (~452—565). The catalytic region is enriched in negatively charged residues (Glu, Asp), which facilitates recognition of polybasic substrates such as the SARS-CoV-2 S protein. The P domain stabilizes the catalytic domain via hydrophobic interactions and is essential for folding and activity [48, 49]. The molecular dynamics results are consistent with Dahms *et al.* [17], who showed that the substrate recognition involves residues in the S1, S2, and S4 pockets (Asp258, Asp306, Glu257, Ser253, Gly255, Tyr308). In present simulations, RMSD values below 0.25 nm indicate that ligand binding does not alter the global fold. The catalytic triad (Asp153–His194–Ser368) remained structurally stable without significant RMSF fluctuations, preserving the active site architecture for 100 ns.

Moderate flexibility was observed in the loop regions near the active site, particularly around Asp153 (140—160), His194 (190—200), and residues Asp258 and Asp306 (250—320), consistent with the conformational adaptability described by Dahms *et al.* [17]. Importantly, the key residues of S1 pocket (Asp258, Asp306), required for recognition of the SARS-CoV-2 S protein, remained stable [40], as did Tyr308 and Tyr313 near the binding cleft [50]. Hydrogen bond analysis confirmed stable ligand binding with robust interactions involving Glu271, Ser311, and Tyr313.

Beyond the catalytic region, all ligands interacted with residues in the cysteine-rich domain,

including Arg490, Asn529, Trp531, and Ala532. Nelfinavir formed hydrogen bonds with Asn529 and Ala532, PI8 engaged Arg490 through hydrogen bonding and π-stacking with Trp531, while remdesivir showed mainly hydrophobic contacts with Trp531. This region, stabilized by conserved disulfide bonds, contributes to the structural integrity; ligand interactions here likely enhance local stabilization without affecting the global structure, consistent with stable RMSD and moderate RMSF values. These findings are consistent with Kolarič *et al.* [40], who reported that extended pocket interactions improved inhibitor stabilization, and with Örd *et al.* [50], who emphasized the role of conformational flexibility in furin function. Thus, the interactions involving the cysteine-rich region may contribute to the enzyme stabilization and potentially modulate substrate recognition.

Conclusions

This study combined molecular docking and 100 ns MD simulations to evaluate the binding stability of nelfinavir, remdesivir, and PI8 to furin. Docking showed that PI8 exhibits the most favorable binding energy due to polar interactions, hydrophobic contacts, and shape complementarity, despite comparable hydrogen bonding in nelfinavir and remdesivir. The MD simulations confirmed the structural stability of all protein-ligand complexes over 100 ns (RMSD < 0.25 nm). Apo furin and the PI8 complex were the most stable, while remdesivir showed moderate stability; nelfinavir exhibited high fluctuations after ~50 ns. Radius of gyration analysis confirmed the preservation of global compactness for all systems. PI8 demonstrated the most favorable and stable binding behavior, supporting its potential as a furin inhibitor.

REFERENCES

1. *Wrapp D, Wang N, Corbett KS, et al., and McLellan JS.* Cryo-EM structure of the 2019-nCoV spike in the prefusion conformation. *Science.* 2020; **367**(6483):1260—3.
2. *Chen Y, Guo Y, Pan Y, Zhao ZJ.* Structure analysis of the receptor binding of 2019-nCoV. *Biochem Biophys Res Commun.* 2020; **525**(1):135—40.
3. *Gross LZF, Sacerdoti M, Piiper A, et al., and Biondi RM.* ACE2, the receptor that enables infection by SARS-CoV-2: biochemistry, structure, allostery and evaluation of the potential development of ACE2 modulators. *ChemMedChem.* 2020; **15**(18):1682—90.
4. *Villoutreix BO, Badiola I, Khatib AM.* Furin and COVID19: structure, function and chemoinformatic analysis of representative active site inhibitors. *Front Drug Discov.* 2022; **2**:899239.
5. *Coutard B, Valle C, de Lamballerie X, et al., and Decroly E.* The spike glycoprotein of the new coronavirus 2019-nCoV contains a furin-like cleavage site absent in CoV of the same clade. *Antiviral Res.* 2020; **176**:104742.
6. *Vankadari N.* Structure of furin protease binding to SARS-CoV-2 spike glycoprotein and implications for potential targets and virulence. *J Phys Chem Lett.* 2020; **11**(16):6655—63.
7. *Seidah NG, Prat A.* The biology and therapeutic targeting of the proprotein convertases. *Nat Rev Drug Discov.* 2012; **11**(5):367—83.
8. *Wu C, Liu Y, Yang Y, et al., and Li H.* Analysis of therapeutic targets for SARS-CoV-2 and discovery of potential drugs by computational methods. *Acta Pharm Sin B.* 2020; **10**(5):766—88.
9. *Lu Y, Hardes K, Dahms SO, et al., and Garten W.* Peptidomimetic furin inhibitor MI-701 in combination with oseltamivir and ribavirin efficiently blocks propagation of highly pathogenic avian influenza viruses and delays high level oseltamivir resistance in MDCK cells. *Antiviral Res.* 2015; **120**:89—100.
10. *Moulard M, Decroly E.* Maturation of HIV envelope glycoprotein precursors by cellular endoproteases. *Biochim Biophys Acta.* 2000; **1469**(3):121—32.
11. *Basak A, Zhong M, Munzer JS, et al., and Seidah NG.* Implication of the proprotein convertases furin, PC5 and PC7 in the cleavage of surface glycoproteins of Hong Kong, Ebola and respiratory syncytial viruses: a comparative analysis with fluorogenic peptides. *Biochem J.* 2001; **353**(Pt 3):537—45.

12. *Bronnimann MP, Calton CM, Chiquette SF, et al., and Campos SK.* Furin Cleavage of L2 during Papillomavirus Infection: Minimal Dependence on Cyclophilins. *J Virol.* 2016; **90**(14):6224—34.
13. *Zhong M, Lin B, Pathak JL, et al., and Wang L.* ACE2 and furin expressions in oral epithelial cells possibly facilitate COVID-19 infection via respiratory and fecal-oral routes. *Front Med (Lausanne).* 2020; **7**:580796.
14. *Osadchuk TV, Shybyryn OV, Kibirev VK.* Chemical structure and properties of low-molecular furin inhibitors. *Ukr Biochem J.* 2016; **88**(6):5—25.
15. *Henrich S, Cameron A, Bourenkov GP, et al., and Than ME.* The crystal structure of the proprotein processing proteinase furin explains its stringent specificity. *Nat Struct Biol.* 2003; **10**(7):520—6.
16. *He Z, Thorrez L, Siegfried G, et al., and Creemers JWM.* The proprotein convertase furin is a pro-oncogenic driver in KRAS and BRAF driven colorectal cancer. *Oncogene.* 2020; **39**(17):3571—87.
17. *Dahms SO, Arciniega M, Steinmetzer T, et al., and Than ME.* Structure of the unliganded form of the proprotein convertase furin suggests activation by a substrate-induced mechanism. *Proc Natl Acad Sci U S A.* 2016; **113**(40): 11196—201.
18. *Hoffmann M, Kleine-Weber H, Schroeder S, et al., and Pöhlmann S.* SARS-CoV-2 cell entry depends on ACE2 and TMPRSS2 and is blocked by a clinically proven protease inhibitor. *Cell.* 2020; **181**(2):271—80.e8.
19. *Simmons G, Gosalia DN, Rennekamp AJ, et al., and Bates P.* Inhibitors of cathepsin L prevent severe acute respiratory syndrome coronavirus entry. *Proc Natl Acad Sci U S A.* 2005; **102**(33):11876—81.
20. *Ivachtchenko AV, Khvat AV, Shkil DO.* Development and prospects of furin inhibitors for therapeutic applications. *Int J Mol Sci.* 2024; **25**(17):9199.
21. *Becker GL, Sielaff F, Than ME, et al., and Steinmetzer T.* Potent inhibitors of furin and furin-like proprotein convertases containing decarboxylated P1 arginine mimetics. *J Med Chem.* 2010; **53**(3):1067—75.
22. *Dufour EK, Denault JB, Hopkins PC, Leduc R.* Serpin-like properties of alpha1-antitrypsin Portland towards furin convertase. *FEBS Lett.* 1998; **426**(1):41—6.
23. *Jiao GS, Cregar L, Wang J, et al., and Thomas G.* Synthetic small molecule furin inhibitors derived from 2,5-dideoxystreptamine. *Proc Natl Acad Sci U S A.* 2006; **103**(52):19707—12.
24. *Xu YM, Inacio MC, Liu MX, Gunatilaka AAL.* Discovery of diminazene as a dual inhibitor of SARS-CoV-2 human host proteases TMPRSS2 and furin using cell-based assays. *Curr Res Chem Biol.* 2022; **2**:100023.
25. *Bestle D, Heindl MR, Limburg H, et al., and Böttcher-Friebertshäuser E.* TMPRSS2 and furin are both essential for proteolytic activation of SARS-CoV-2 in human airway cells. *Life Sci Alliance.* 2020; **3**(9):e202000786.
26. *Carranza-Aranda AS, Diaz-Palomera CD, Lepe-Reynoso E, et al., and Viera-Segura O.* Evaluation of potential furin protease inhibitory properties of pioglitazone, rosiglitazone, and pirfenidone: an in silico docking and molecular dynamics simulation approach. *Curr Issues Mol Biol.* 2024; **46**(8):8665—84.
27. *Jorkesh A, Rothenberger S, Baldassar L, et al., and Pasquato A.* Screening of small-molecule libraries using SARS-CoV-2-derived sequences identifies novel furin inhibitors. *Int J Mol Sci.* 2024; **25**(10):5079.
28. *Saih A, Baammi S, Charoute H, et al., and Kettani A.* Repositioning of Furin inhibitors as potential drugs against SARS-CoV-2 through computational approaches. *J Biomol Struct Dyn.* 2026; **44**(4):1681—95.
29. *Lahlil R, Calvo F, Khatib AM.* The potential anti-tumorigenic and anti-metastatic side of the proprotein convertases inhibitors. *Recent Pat Anticancer Drug Discov.* 2009; **4**(1):83—91.
30. *Søndergaard CR, Olsson MH, Rostkowski M, Jensen JH.* Improved treatment of ligands and coupling effects in empirical calculation and rationalization of pKa values. *J Chem Theory Comput.* 2011; **7**(7):2284—95.
31. *Trott O, Olson AJ.* AutoDock Vina: improving the speed and accuracy of docking with a new scoring function, efficient optimization, and multithreading. *J Comput Chem.* 2010; **31**(2):455—61.
32. *Kochnev Y, Durrant JD.* FPocketWeb: protein pocket hunting in a web browser. *J Cheminform.* 2022; **14**(1):58.
33. *Schrödinger L, Delano W.* PyMOL. The PyMOL Molecular Graphics System, Version 2. Schrödinger, LLC: New York, NY, USA. 2020.
34. BIOVIA, Dassault Systèmes. Discovery Studio Client 2024. Dassault Systèmes, San Diego, CA, USA, 2024.
35. GROMACS 2024.4 Development Team. GROMACS user guide for version 2024.4. 2024.
36. *Zoete V, Cuendet MA, Grosdidier A, Michielin O.* SwissParam: a fast force field generation tool for small organic molecules. *J Comput Chem.* 2011; **32**(11):2359—68.

37. *Darden T, York D, Pedersen L.* Particle mesh Ewald: An N log (N) method for Ewald sums in large systems. *J Chem Phys.* 1993; **98**:10089.
38. *Liu Y, Yang X, Gan J, et al., and Cao Y.* CB-Dock2: improved protein-ligand blind docking by integrating cavity detection, docking and homologous template fitting. *Nucleic Acids Res.* 2022; **50**(W1):W159–W164.
39. *Becker GL, Lu Y, Hardes K, et al., and Steinmetzer T.* Highly potent inhibitors of proprotein convertase furin as potential drugs for treatment of infectious diseases. *J Biol Chem.* 2012; **287**(26):21992—2003.
40. *Kolarič A, Ravnik V,* Štumpf *Horvat S, et al., and Bren U.* Identification of furin protease small-molecule inhibitor with a 1,3-Thiazol-2-ylaminosulfonyl scaffold. *Pharmaceuticals (Basel).* 2025; **18**(2):273.
41. *Khmil NV, Shestopalova AV, Kolesnikov VG.* In silico analysis of binding sites for potential inhibitors targeting the complex of furin protease and the SARS-CoV-2 spike protein. *Biophysical Bulletin.* 2025; (54):9—26.
42. *Tyndall JD, Reid RC, Tyssen DP, et al., and Fairlie DP.* Synthesis, stability, antiviral activity, and protease-bound structures of substrate-mimicking constrained macrocyclic inhibitors of HIV-1 protease. *J Med Chem.* 2000; **43**(19):3495—504.
43. *Kaldor SW, Kalish VJ, Davies JF 2nd, et al., and Tatlock JH.* Viracept (nelfinavir mesylate, AG1343): a potent, orally bioavailable inhibitor of HIV-1 protease. *J Med Chem.* 1997; **40**(24):3979—85.
44. *Gaucher B, Rouquayrol M, Roche D, et al., and Vierling P.* Prodrugs of HIV protease inhibitors-saquinavir, indinavir and nelfinavir-derived from diglycerides or amino acids: synthesis, stability and anti-HIV activity. *Org Biomol Chem.* 2004; **2**(3):345—57.
45. *Ghosh AK, Osswald HL, Prato G.* Recent Progress in the Development of HIV-1 Protease Inhibitors for the Treatment of HIV/AIDS. *J Med Chem.* 2016; **59**(11):5172—208.
46. *Gordon CJ, Tchesnokov EP, Woolner E, et al., and Götte M.* Remdesivir is a direct-acting antiviral that inhibits RNA-dependent RNA polymerase from severe acute respiratory syndrome coronavirus 2 with high potency. *J Biol Chem.* 2020; **295**(20):6785—97.
47. *Kokic G, Hillen HS, Tegunov D, et al., and Cramer P.* Mechanism of SARS-CoV-2 polymerase stalling by remdesivir. *Nat Commun.* 2021; **12**(1):279.
48. *Lipkind GM, Zhou A, Steiner DF.* A model for the structure of the P domains in the subtilisin-like prohormone convertases. *Proc Natl Acad Sci U S A.* 1998; **95**(13):7310—5.
49. *Zhou A, Martin S, Lipkind G, et al., and Steiner DF.* Regulatory roles of the P domain of the subtilisin-like prohormone convertases. *J Biol Chem.* 1998; **273**(18):11107—14.
50. Örd *M, Faustova I, Loog M.* The sequence at Spike S1/S2 site enables cleavage by furin and phospho-regulation in SARS-CoV2 but not in SARS-CoV1 or MERS-CoV. *Sci Rep.* 2020; **10**(1):16944.

Received: 27.04.2026
Accepted: 16.06.2026
Published: 25.06.2026

Н.В.Хміль[1, 2], *А.В. Шестопалова*[1]

[1] Інститут радіофізики та електроніки ім. О.Я. Усикова НАН України
вул. Академіка Проскури, 12, Харків, Україна, 61085
[2] Харківський національний університет радіоелектроніки
просп. Науки, 14, Харків, Україна, 61166
nataliia.khmil@nure.ua

ВПЛИВ ПРОТИВІРУСНИХ ПРЕПАРАТІВ ТА ПЕПТИДОМІМЕТИЧНОГО ІНГІБІТОРА НА КОНФОРМАЦІЙНУ СТАБІЛЬНІСТЬ ФУРИНУ: МОЛЕКУЛЯРНИЙ ДОКІНГ ТА МОЛЕКУЛЯРНО-ДИНАМІЧНЕ МОДЕЛЮВАННЯ

Фурин є ключовою протеазою хазяїна, яка бере участь у протеолітичній активації шипоподібного білка SARS-CoV-2 в ділянці розщеплення S1/S2, сприяючи злиттю вірусної та клітинної мембран, що робить його привабливою мішенню для розробки противірусних препаратів. ***Мета.*** Оцінити конформаційну стабільність та поведінку зв'язування фурину в комплексі з нелфінавіром, ремдесивіром та макроциклічним пептидоміметичним інгібітором 8 (PI8) за допомогою обчислювальних підходів. ***Методи.*** Молекулярний докінг та 100-нс молекулярно-динамічне моделювання були застосовані для визначення режимів зв'язування лігандів та оцінки структурної стабільності комплексів фурин-ліганд. ***Результати.*** Докінговий аналіз визначив PI8 як енергетично найвигіднішу сполуку (–9,1 ккал/моль), що формує стабільні взаємодії в каталітичному сайті, тоді як нелфінавір і ремдесивір демонстрували дещо менш сприятливі енергії зв'язування (–8,7 та –8,9 ккал/моль, відповідно). Молекулярно-динамічне моделювання підтвердило структурну стабільність усіх комплексів протягом 100-нс траєкторії, що свідчить про надійність передбачених режимів зв'язування. ***Висновки.*** Молекулярний докінг та молекулярно-динамічне моделювання забезпечують надійну основу для ідентифікації та характеристики потенційних інгібіторів фурину.

***Ключові слова*:** фурин, противірусні препарати, пептидоміметичний інгібітор 8, шипоподібний білок SARS-CoV-2, молекулярний докінг, молекулярно-динамічне моделювання.